

ACOUSTICAL LETTER

Tube-type double-parabolic-reflector ultrasonic transducer (T-DPLUS)

Kyohei Yamada[1,*], Kang Chen[1], Takasuke Irie[2], Takashi Iijima[3], Susumu Miyake[1] and Takeshi Morita[1,†]

[1]*The University of Tokyo, Tokyo, 113–8656 Japan*
[2]*Microsonic Co., Ltd., Kokubunji, 185–0012 Japan*
[3]*National Institute of Advanced Industrial Science and Technology, Tsukuba, 305–8569 Japan*

(*Received 8 April 2022, Accepted for publication 13 May 2022*)

Keywords: Ultrasonic transducer, Parabolic focusing, Minimally invaseive treatment, Acoustic waveguide, DPLUS

1. Introduction

There is no doubt that a variety of ultrasonic applications is supported by ultrasonic transducer technology. One of the most commonly used ultrasonic transducers is the bolt-clamped Langevin-type transducer (BLT). The BLT is a high-power transducer in which laminated piezoelectric ceramics are sandwiched between metal blocks and tightened with a bolt. BLTs are widely used in high-power ultrasound devices, such as actuators [1], cleaners [2], and grinders [3]. However, a BLT has only a single working frequency lower than several hundred kilohertz, which limits the application possibilities. Recently, Chen *et al.* studied a double-parabolic-reflector ultrasonic transducer (DPLUS) [4–7], which consists of a lead zirconate titanate (PZT) ring, double-parabolic reflectors (1st and 2nd reflectors), which share the same focal point, and a thin waveguide. The 1st reflector focuses the incident plane wave from the PZT ring, and the 2nd reflector reflects the ultrasound and turns it into an in-phase plane wave, which propagates into the thin waveguide. This process enhances the energy density of the ultrasound because the size of the 2nd reflector is smaller than that of the 1st reflector. The enhanced ultrasound is finally radiated from the tip of the thin waveguide. DPLUS can realize wideband (20 kHz to 2.5 MHz), high-intensity (several megapascals) ultrasound generation near the tip of the thin waveguide. These characteristics are difficult to achieve with conventional transducers containing BLTs. Hence, DPLUS expands potential applications of ultrasonic technology in various fields, such as ultrasound therapeutics [7], medical imaging, and ultrasonic tweezers.

One of the most promising applications of DPLUS is minimally invasive treatment (MIT), in which a thin needle is inserted through a surgical incision into the treatment target, and energy, such as radiofrequency, microwave, laser, or ultrasound, is directly delivered to ablate the target [7]. Ultrasound-based MIT has multiple treatment mechanisms, such as cavitation, direct mechanical impact, and thermal effects, according to the tissue type and working frequency [8,9], and various ultrasound applicators have been studied [10,11]. Because DPLUS has characteristics suitable for MIT, high-power and localized ultrasound through a thin waveguide, MIT with DPLUS is promising [7]. However, in actual use, conventional DPLUS may be challenging for sensing physical phenomena near the tip, such as sound pressure, temperature, and optical imagery. Therefore, for MIT with DPLUS, it is necessary to make extra surgical incisions and insert sensors to perceive the condition of the treatment target, similar to the use of MIT with other acoustic waveguide applicators [9]. Multiple incisions can cause more pain and risk for patients. Moreover, multiple sensors may be difficult to align correctly to the treatment target.

To solve this problem, we propose a tube-type DPLUS (T-DPLUS), where the waveguide is hollow so that sensors can be integrated inside it. This structure allows T-DPLUS to have various advantages that were not possible with conventional DPLUS. For the example of MIT, T-DPLUS realizes a single small incision area and allows the easy positioning of sensors. In addition, T-DPLUS can also be used as a puncture needle-type ultrasonic microscope, which can help diagnose tissue by endoscopic ultrasonography [12] by inserting a sound pressure sensor, such as a hydrophone, inside it. This microscopic application is too complex using conventional DPLUS because a sound pressure sensor cannot be affixed to the DPLUS, and the DPLUS itself may have difficulty acquiring acoustic signals. When we use the PZT ring of DPLUS to catch the reflected signal, the signal propagates the amplification mechanism inversely, and it significantly attenuates before it reaches the PZT ring. In this study, we designed double-reflector structures for T-DPLUS and compared them in a simulation and experiment.

2. Method

First, we consider simply hollowing out the DPLUS along the central axis while maintaining its shape, as shown in Fig. 1(a). We name this structure Model 1. The ultrasound reflected by the 1st reflector propagates toward the focal point, just as in the conventional DPLUS. However, because the focal point is in the hollow part, the ultrasound is reflected and refracted at the boundary between the hollow and metal part; thus, the ultrasound cannot focus on the focal point. Therefore, it was expected that Model 1 would not work well.

To solve this problem, we next designed another reflector structure, Model 2, as shown in Fig. 1(b). We moved the focal point into the metal part to avoid the undesired reflection and refraction. This structure is designed as the following procedure. First, in Fig. 1(c), the conventional double-parabolic reflector is the solid of revolution when the pink area

*e-mail: yamada-kyohei355@g.ecc.u-tokyo.ac.jp
†e-mail: morita@pe.t.u-tokyo.ac.jp
[doi:10.1250/ast.43.287]

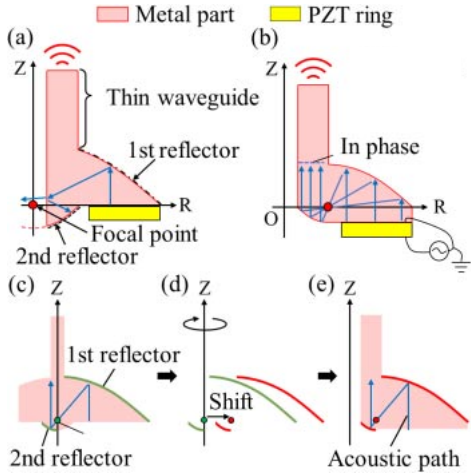

Fig. 1 Structures of T-DPLUS: (a) simple hollow structure, Model 1, (b) proposed structure, Model 2, (c)–(e) design process of Model 2.

spins around the z-axis. By translating the double-parabolic curves of conventional DPLUS in the direction perpendicular to the z-axis, as shown in Fig. 1(d), we can generate the new solid of revolution, in which the focal point is not on the z-axis. Finally, this structure is hollowed out along the z-axis, as shown in Fig. 1(e). The amplifying mechanism of Model 2 is shown in Fig. 1(b). First, Model 2 focuses the plane-wavefront ultrasound emitted from the PZT ring into the focal point by the first reflection at the 1st reflector. Then, it generates the amplified plane-wavefront ultrasound by the second reflection at the 2nd reflector. The amplified ultrasound propagates into the thin waveguide and is finally radiated from the tip.

T-DPLUS consists of a PZT ring and a metal part. For the PZT ring, PZT MT-5H (NGK Spark Plug Co., Ltd.) was selected because of its high d33 value, 619×10^{-12} m/V, which leads to a high vibration velocity. As for the other properties of PZT MT-5H, the electromechanical coupling coefficient k_t is 53%, and the mechanical quality factor Q_m is 61. The elastic compliance s_{ij}^E, piezoelectric constant d_{mn}, and relative permittivity $\varepsilon_{mn}^\mathrm{T}/\varepsilon_0$ are represented by Eqs. (1), (2), and (3), respectively.

$$[s_{ij}^\mathrm{E}] = \begin{bmatrix} 16.8 & -5.9 & -8.3 & 0 & 0 & 0 \\ -5.9 & 16.8 & -8.3 & 0 & 0 & 0 \\ -8.3 & -8.3 & 21.8 & 0 & 0 & 0 \\ 0 & 0 & 0 & 41.7 & 0 & 0 \\ 0 & 0 & 0 & 0 & 41.7 & 0 \\ 0 & 0 & 0 & 0 & 0 & 45.5 \end{bmatrix} \times 10^{-12}\,\mathrm{m^2/N}, \tag{1}$$

$$[d_{mn}] = \begin{bmatrix} 0 & 0 & 0 & 0 & 841 & 0 \\ 0 & 0 & 0 & 841 & 0 & 0 \\ -285 & -285 & 619 & 0 & 0 & 0 \end{bmatrix} \times 10^{-12}\,\mathrm{m/V}, \tag{2}$$

$$\left[\frac{\varepsilon_{nm}^\mathrm{T}}{\varepsilon_0}\right] = \begin{bmatrix} 3{,}500 & 0 & 0 \\ 0 & 3{,}500 & 0 \\ 0 & 0 & 3{,}400 \end{bmatrix}. \tag{3}$$

The outer diameter (OD) of the PZT ring was 40 mm, the inner diameter (ID) was 18 or 16 mm, and the thickness was 1.1 mm. The difference in ID (18 mm or 16 mm) had little effect on the characteristics of T-DPLUS because the resonant frequency of the thickness mode (1.74 MHz) did not change, and the difference in area is only 5%.

For the metal part, duralumin (A2017) was selected because it can be easily machined. The metal part consisted of double reflectors and a thin tubular waveguide. The double reflectors consist of the 1st reflector (OD: 40 mm, ID: 2 mm) and the 2nd reflector (OD: 6 mm, ID: 2 mm). In Model 1, the 1st and 2nd reflector shapes are represented by Eqs. (4) and (5), respectively, and the focal point of these parabolas is $(0, 0)$. In Model 2, the 1st and 2nd reflector shapes are represented by Eqs. (6) and (7), respectively, and the focal point of these parabolas is the point $(0, 3)$. Note that Z is the axial coordinate and R is the radial coordinate (both in millimeters), as shown in Fig. 1.

$$Z = -\frac{R^2}{40} + 10 \ (2.5 \le R \le 20), \tag{4}$$

$$Z = \frac{R^2}{6} - 1.5 \ (1.0 \le R \le 3.0), \tag{5}$$

$$Z = -\frac{(R-3)^2}{34} + 8.5 \ (2.5 \le R \le 20), \tag{6}$$

$$Z = \frac{(R-3)^2}{4} - 1.0 \ (1.0 \le R \le 3.0). \tag{7}$$

The thin waveguide was thicker and shorter than that of a conventional DPLUS for easy processing; the OD was 5 mm, the ID was 2 mm, and the length was 10 mm in Models 1 and 2.

Prototypes of Models 1 and 2 were fabricated using the above materials and dimensions. The metal part was machined as one part for the prototypes. A photograph of Model 2 is shown in Fig. 2; Figs. 2(a), 2(b), and 2(c) show the front, side, and back views, respectively. For mounting to a fixed position, T-DPLUS has a flange 0.5 mm thick on its periphery and is bolted to a brass fixture with a duralumin mounting ring in between, as shown in Fig. 2(b). The metal part and PZT ring were bonded by epoxy adhesive. The adhesive layer is sufficiently thin that the electrodes of the PZT ring and the metal part are conductive. The ground wire was electrically connected to the bonded surface of the PZT ring through the brass fixture, the duralumin mounting ring, and the metal part, as shown in Fig. 2(b). The hot wire was soldered on the other surface of the PZT ring, as shown in Fig. 2(c).

The output ultrasound from Models 1 and 2 was simulated using the finite element method (FEM) and measured using the prototypes. The medium for ultrasonic irradiation was water, of which acoustic impedance is close to that of biological tissue. First, the sound pressure distribution in water was simulated using the FEM-based software PZFlex

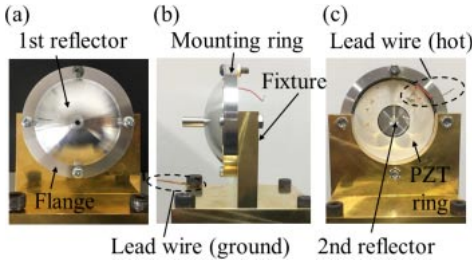

Fig. 2 Prototype of T-DPLUS (Model 2): (a) front view, (b) side view, (c) back view.

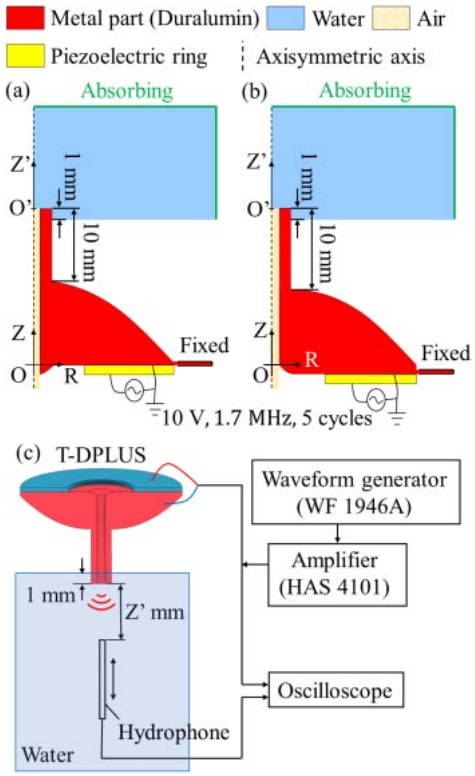

Fig. 3 Setups for a simulation and experiment: simulation model for (a) Model 1 and (b) Model 2, (c) sound pressure measurement system.

(Weidlinger Associates, Los Altos, CA). The Models 1 and 2 simulations were constructed as axisymmetric models, as shown in Figs. 3(a) and 3(b). Models 1 and 2 were fixed at the thin flange, and their thin waveguide tips were immersed in water to a depth of 1 mm. The input voltage was applied between the hot and ground electrodes of the PZT rings. The attenuation in the metal and water was neglected. As shown in Figs. 3(a) and 3(b), the upper and right side of the water was an absorbing boundary condition, and the tube was filled with air. The mesh size was 50 µm, which is smaller than 1/15 of the wavelength in water. The simulated time was 80 µs, long enough for the ultrasound to propagate deep into the water. The applied signal was a 5-cycle sinusoidal wave burst. The applied peak-to-peak voltage was 10 V, and the driving frequency was 1.7 MHz, which was close to the resonant frequency of the thickness mode of the PZT ring.

Next, sound pressure measurements with the prototypes were performed using the measurement system shown in Fig. 3(c). The signal generated by a waveform generator (WF 1946A, NF Corp.) was amplified by a power amplifier (HAS 4101, NF Corp.) and applied to T-DPLUS. The applied signal was a 5-cycle burst of sinusoidal waves. The peak-to-peak voltage was 10 V, and the driving frequency was 1.7 MHz. T-DPLUS was inserted 1 mm from the tip, and ultrasound was emitted into the water. The water used in this experiment was tap water poured into an acrylic tank 200 mm wide × 200 mm deep × 200 mm high. The sound pressure in the water was measured by a needle hydrophone (HNR-0500, ONDA). The hydrophone body diameter was 2.5 mm, and the diameter of the PZT, which senses the signal at the hydrophone tip, was 0.5 mm. The hydrophone was held vertically and fixed to a z-stage. The Z' position of the hydrophone was adjusted, and the sound pressure was measured at each point where the distance Z' from the T-DPLUS tip was from 0.5 to 15 mm along the central axis of T-DPLUS. The signal from the hydrophone and the applied voltage were acquired by the oscilloscope.

3. Results and discussion

Figures 4(a) and 4(b) show the simulated overall maximum sound pressure distribution. At each point in the PZT ring, metal part, and water, a burst signal of sound pressure was observed, and its maximum zero-to-peak amplitude was represented by a color map. In Model 1, as shown in Fig. 4(a), the sound pressure at the focal point is low, 0.61 kPa, indicating that the ultrasound cannot be focused due to the reflection and refraction at the inner surface. In contrast, in Model 2, shown in Fig. 4(b), the sound pressure near the focal point is high, 870 kPa, indicating that the ultrasonic waves are focused as intended.

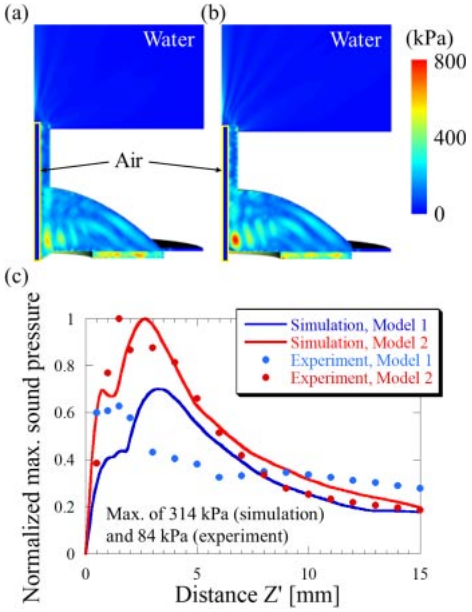

Fig. 4 Results: the overall maximum sound pressure distribution of (a) Model 1 and (b) Model 2, (c) normalized maximum acoustic pressure distribution along the Z' axis in water.

The sound pressure on the Z'-axis in the experiment is shown in Fig. 4(c). At each point along the distance $Z' =$ 0.5–15 mm, a burst signal of sound pressure was observed, and the maximum zero-to-peak amplitude was normalized and plotted against the distance Z'. The sound pressure distribution obtained in the simulation is also plotted for comparison. In Model 2, the measured pressure distribution is consistent with the simulated distribution. In the experiment, the highest acoustic pressure was 84 kPa at the distance $Z' =$ 1.5 mm, and the 2nd- and 3rd-highest pressures normalized by 84 kPa were 0.88 at $Z' = 3$ and 0.87 at $Z' = 2$ mm, respectively. Because the highest simulated sound pressure was obtained at $Z' = 2.7$ mm, the highest acoustic pressure was obtained at a similar position in the experiment and simulation. The acoustic pressure decreases toward 0 as the distance becomes closer than 1.5 mm, while the conventional DPLUS has a maximum sound pressure at $Z' = 0$ [5]. This difference is because, in T-DPLUS, the ultrasound is not irradiated from the center on the waveguide tip, which is a hollow part, so the transmitted ultrasound needs some distance to converge. The acoustic pressure decreased as the distance became larger than 3 mm because the ultrasound was diffusively attenuated. In contrast, the measured pressure distribution of Model 1 was not so consistent with that of the simulation. In Model 1, the highest normalized sound pressure was 0.70 at the distance $Z' = 1.5$ mm in the experiment and 0.62 at $Z' = 3.3$ mm in the simulation. The highest normalized sound pressure is similar, but the observed distance Z' is different. This is probably because the water level in the tube differed 1 mm at most from the simulation because of surface tension. We did another simulation and found that the pressure distribution shape varies with the water level in the tube, but the maximum value does not change significantly. We are studying this effect in detail. By comparing the measured highest sound pressure, Model 2 realized sound pressure 1.6 times as high as that of Model 1. This result suggests that Model 2 realizes excellent performance due to its double-reflector structure. As for the absolute sound pressure value, the highest sound pressure was 314 kPa in the simulation and 84 kPa in the experiment. The lower sound pressure in the experiment might be due to the difference between the simulation setup and the experimental condition, such as attenuation in the metal part and water, sound pressure distribution on the hydrophone tip, and angular error of the hydrophone.

In this work, we proposed T-DPLUS and verified that the proposed structure Model 2 has excellent performance. However, Model 2 did not generate overwhelmingly large sound pressure in water compared to Model 1, although the sound pressure generated by Model 2 was higher than that by Model 1. This is probably because the length of the thin waveguide in this study is so short that the advantage of the Model 2 reflectors is not fully exploited. Next, we plan to analyze how the waves amplified by the Model 2 reflectors propagate through a long thin waveguide.

Acknowledgments

This work was supported by JSPS KAKENHI Grant Numbers JP20H02097 and JP21KK0065.

References

[1] M. K. Kurosawa, O. Kodaira, Y. Tsuchitoi and T. Higuchi, "Transducer for high speed and large thrust ultrasonic linear motor using two sandwich-type vibrators," *IEEE Trans. Ultrason. Ferroelectr. Freq. Control*, **45**, 1188–1195 (1998).

[2] T. Tou, Y. Hamaguti, Y. Maida, H. Yamamori, K. Takahashi and Y. Terashima, "Properties of $(Bi_{0.5}Na_{0.5})TiO_3$–$BaTiO_3$–$(Bi_{0.5}Na_{0.5})(Mn_{1/3}Nb_{2/3})O_3$ lead-free piezoelectric ceramics and its application to ultrasonic cleaner," *Jpn. J. Appl. Phys.*, **48**, 07GM03 (2009).

[3] Y. J. Choi, K. H. Park, Y. H. Hong, K. T. Kim, S. W. Lee and H. Z. Choi, "Effect of ultrasonic vibration in grinding; horn design and experiment," *Int. J. Precis. Eng. Manuf.*, **14**, 1873–1879 (2013).

[4] K. Chen, T. Irie, T. Iijima and T. Morita, "Acoustic focusing to the waveguides utilizing double parabolic reflectors," *Appl. Phys. Lett.*, **114**, 072902 (2019).

[5] K. Chen, T. Irie, T. Iijima and T. Morita, "Double-parabolic-reflectors acoustic waveguides for high-power medical ultrasound," *Sci. Rep.*, **9**, 18493 (2019).

[6] K. Chen, T. Irie, T. Iijima and T. Morita, "Wideband multimode excitation by a double-parabolic-reflector ultrasonic transducer," *IEEE Trans. Ultrason. Ferroelectr. Freq. Control*, **67**, 1620–1631 (2020).

[7] K. Chen, T. Irie, T. Iijima and T. Morita, "Double-parabolic-reflectors ultrasonic transducer with flexible waveguide for minimally invasive treatment," *IEEE Trans. Biomed. Eng.*, **68**, 2965–2973 (2021).

[8] B. J. O'Daly, E. Morris, G. P. Gavin, J. M. O'Byrne and G. B. McGuinness, "High-power low-frequency ultrasound: A review of tissue dissection and ablation in medicine and surgery," *J. Mater. Process. Technol.*, **200**, 38–58 (2008).

[9] B. J. Jarosz, "Feasibility of ultrasound hyperthermia with waveguide interstitial applicator," *IEEE Trans. Biomed. Eng.*, **43**, 1106–1115 (1996).

[10] C. J. Diederich and K. Hynynen, "Ultrasound technology for hyperthermia," *Ultrasound Med. Biol.*, **25**, 871–887 (1999).

[11] C. J. Diederich, W. H. Nau and P. R. Stauffer, "Ultrasound applicators for interstitial thermal coagulation," *IEEE Trans. Ultrason. Ferroelectr. Freq. Control*, **46**, 1218–1228 (1999).

[12] M. Yoshizawa, R. Emoto, H. Kawabata, T. Irie, K. Itoh and T. Moriya, "Development of scanning method for puncture needle-type ultrasonography," *Jpn. J. Appl. Phys.*, **48**, 07GK12 (2009).